Research

Check for updates

Debonding waves in gel thin films

Xianmin Xu[1], M. Carme Calderer[2], Masao Doi[3] and Duvan Henao[4]

[1]LSEC, Institute of Computational Mathematics and Scientific/Engineering Computing, NCMIS, Academy of Mathematics and Systems Science, Chinese Academy of Sciences, Beijing 100190, People's Republic of China
[2]School of Mathematics, University of Minnesota, Minneapolis, MN 55455, USA
[3]Center of Soft Matter Physics and its Applications, Beihang University, 37 Xueyuan Road, Beijing 100191, People's Republic of China
[4]Faculty of Mathematics, Pontificia Universidad Católica de Chile, Vicuña Mackenna 4860, Santiago, Chile

MCC, 0000-0002-9117-7439

We develop a mathematical model for the sliding of a gel sheet adhered to a moving substrate. The sliding takes place by the motion of detached region between the gel sheet and the substrates, i.e. the propagation of a Schallamach wave. Efficient numerical methods are developed to solve the problem. Numerical examples illustrate that the model can describe the Schallamach wave and are consistent with the existing experiments qualitatively.

1. Introduction

Sliding friction of soft material on substrates is of critical importance in many applications [1,2]. For example, the friction of rubber on solid surfaces is important to study the friction between car tyres and roads. The sliding of soft materials on rigid substrates has also been studied as a model for earthquake [3]. Even though there are many studies for the sliding friction problems, e.g. in [4–12], many aspects of the phenomenon are still not well understood.

In soft materials, the softness of the material and the strong adhesion between the material and the substrate causes a sliding behaviour different from those of hard materials. When a soft material is slid relative to the
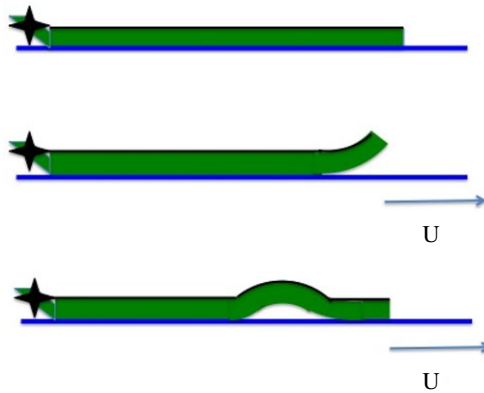
Figure 1. The shape changes of a gel sheet on a sliding substrate. The gel sheet is fixed at the left end and the substrate moves right with constant speed. A detached region may appear in the right end and moves left. (Online version in colour.)

substrate, part of the material is detached from the substrate and the detached part moves, creating the overall sliding. The motion of the detached region is called Schallamach waves [13] and is considered to be one main mechanism of the sliding friction for fast sliding of rubbers. Other important mechanisms include the periodic stick–slip behaviour, which have been studied extensively in fault dynamics (e.g. [14–16]).

Experimental study of the Schallamach wave has been done mostly for the friction of a curved surface of a soft material sliding over a flat rigid substrate [4,7,17]. Though this is a typical situation of sliding of tires, analysis of the phenomena becomes involved as it requires the analysis of nonlinear elasticity in three dimensions.

Yamaguchi *et al.* studied the Schallamach wave for a simple situation as shown in figure 1 [18]. Here a soft gel sheet is sliding on a substrate. A thin inextensible plastic film is adhered on the upper surface of the sheet. One end of the sheet is fixed, and the glass substrate is sliding relative to the sheet. Due to the adhesion between the gel and the glass, the sheet cannot slip on glass when it is attached to the substrate. The relative motion between the sheet and the substrate can take place via the Schallamach wave, the motion of the detached region created at the free end moves towards the fixed end.

Yamaguchi *et al.* observed the spatio-temporal patterns of the detached regions [18,19], and reported that the pattern changes from regular to chaotic when the velocity of the substrate decreases. In regular motions, the measured friction force oscillates periodically. They reported that the velocity V_{wave} of the detached regions increases with the increases of the substrate velocity v_w, following a power law $V_{wave} \propto v_w^\alpha$. Yamaguchi *et al.* conducted a scaling analysis for the regular wave assuming simple geometry of the detached regions.

In this paper, we conduct a more detailed analysis for the phenomenon reported by Yamaguchi *et al.* based on the nonlinear analysis for the bending of the gel sheet. We first derive a reduced elastic model for the gel sheet which has an inextensible upper surface from a nonlinear elastic bulk energy. The reduced energy describes the shear and bending energy stored in the sheet and determines the shape of the detached regions of the thin sheet. The Euler–Lagrange equations are derived for the energy functional in the detached regions. We then derive a dynamic model for the motion of the detachment regions (Schallamach wave) using the Onsager principle. The model describes the whole dynamic process of the stick–slip motion of the gel sheet. We also develop numerical methods for both the static and dynamic problems. Numerical examples show that the model can describe the Schallamach wave of the gel sheet very well and the numerical results fit with the experiments quantitatively in the regular motion regime.

The structure of the paper is as follows. In §2, we derive a reduced elastic model for the gel sheet. In §3, we derive the Euler–Lagrange equations for the elastic model and do some asymptotic analysis. In §4, we propose a dynamic model for the detachment motion of the thin

sheet by using the Onsager principle. In §5, we develop some numerical schemes for both the static and the dynamic problems. Numerical results are illustrated in §6. The results show that the model can describe the Schallamach wave in the sliding of the sheet on the substrate. Some conclusion remarks are given in the last section.

2. A reduced elastic model for a bending gel sheet

In a sliding gel sheet, some parts detach from the substrate. In this section, we derive a reduced elastic model for a detached region.

(a) The reduced energy

As shown in figure 2, we assume the upper surface of an elastic sheet is inextensible and the sheet is sheared in right direction from the bottom. When the shear is strong enough, the sheet will bend upward and detach from the substrate. The deformation of the elastic gel sheet is determined by minimizing the elastic energy stored in it.

To derive a reduced elastic model, we first characterize the deformation of the elastic sheet. Suppose the thickness of the sheet is H and the length of the detached region is l. Denote the reference domain of the region as $[x_0, x_1] \times [0, H]$. Since the upper surface of the sheet is inextensible, we first describe its deformation. Let $s \in (x_0, x_1)$ be the arc length parameter of the upper surface. The deformation of the upper surface can be described solely by a height function $h(s)$. The generic point (s, H) on the upper surface in the reference domain is mapped to a point $(X(s), h(s))$, where $X(s)$ can be computed out by using the inextensibility of the upper surface.

Since the sheet is very thin, we could assume that its section line, which is orthogonal to the upper surface in the reference domain, is still a straight line after deformation. Suppose the unit normal vector of the deformed upper surface is given by $\mathbf{n}(s)$ and the unit tangential vector is given by $\boldsymbol{\tau}(s)$. In the deformed domain, the section line may deviate from the normal direction $\mathbf{n}$, as shown in figure 2. The deviation of the section can be described by a shear function $\gamma(s)$. For any point in the reference domain $(s, y) \in [x_0, x_1] \times [0, H]$, it is mapped to a point

$$(X(s), h(s)) + (H - y)\mathbf{n} + \gamma(s)(H - y)\boldsymbol{\tau}.$$

For simplicity, we denote $(u(s, y), v(s, y))$ as the point in the deformed domain corresponding to a point (s, y) in the reference domain. Then

$$(u(s, y), v(s, y)) = (X(s), h(s)) + (H - y)\mathbf{n} + \gamma(s)(H - y)\boldsymbol{\tau}.$$

Then we have $u(s, H) = X(s)$ and $v(s, H) = h(s)$. Denote by

$$\mathbf{r}(s) = (u(s, H), v(s, H)) = (X(s), h(s)), \tag{2.1}$$

the position vector in the deformed upper surface of the material point initially located at (s, H). Since the upper surface is inextensible, we have

$$(\partial_s u(s, H))^2 + (h'(s))^2 = |\mathbf{r}'(s)|^2 = 1.$$

Thus, $\mathbf{r}'$ is actually the unit tangential vector $\boldsymbol{\tau}$ on the upper surface. As stated above, we have assumed that the deformation of the section line is still straight in the thin sheet, as shown in figure 2. Hence, the vector joining the point (s, H) with its corresponding point on the bottom surface is mapped to

$$\mathbf{p} = H\mathbf{n}(s) + H\gamma(s)\mathbf{r}'(s). \tag{2.2}$$

Then the deformation of the thin sheet can be reformulated as

$$(u, v) = \mathbf{r}(s) + \frac{H - y}{H}\mathbf{p}$$
$$= \mathbf{r}(s) + (H - y)(\mathbf{n}(s) + \gamma(s)\mathbf{r}'(s)). \tag{2.3}$$
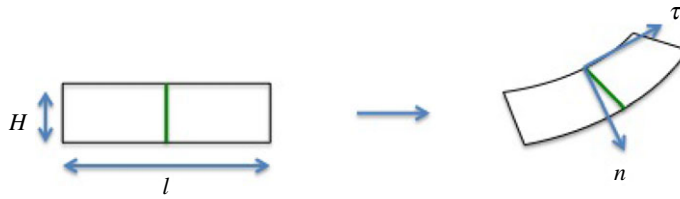
Figure 2. The deformation of a detached region of a thin elastic sheet. (Online version in colour.)

We suppose that the elasticity energy density is given by

$$W(\mathbf{F}) = \frac{G}{2}(|\mathbf{F}|^2 - |\mathbf{I}|^2) + \lambda\phi(\det\mathbf{F}),$$

for some function ϕ satisfying

$$\phi(1) = 0, \quad \phi'(1) = -G, \quad \phi''(1) = G + \lambda,$$

where G and λ are the Lamé moduli of the material. Here $\mathbf{F} = \begin{pmatrix} \partial_s u & \partial_y u \\ \partial_s v & \partial_y v \end{pmatrix}$ is the deformation tensor. When the sheet is almost incompressible, $\det\mathbf{F} \approx 1$, we have

$$W(\mathbf{F}) \approx \frac{G}{2}(|\mathbf{F}|^2 - |\mathbf{I}|^2). \tag{2.4}$$

It corresponds to a neo-Hookean material. Here we assume that the energy density is zero when the material does not deform. Direct computation gives

$$W(\mathbf{F}) = \frac{G}{2}\left(|\mathbf{r}' + (H - y)(\mathbf{n} + \gamma\mathbf{r}')'|^2 + |\mathbf{n} + \gamma\mathbf{r}'|^2 - 2\right)$$

$$= \frac{G}{2}\left(2(H - y)\mathbf{r}' \cdot (\mathbf{n} + \gamma\mathbf{r}')' + (H - y)^2|(\mathbf{n} + \gamma\mathbf{r}')'|^2 + \gamma^2\right).$$

Then the reduced energy density w for the elastic sheet is obtained by the integral average of W in the cross section, given by

$$w = \int_0^H W(\mathbf{F})\,\mathrm{d}y = \frac{G}{2}\left(\gamma^2 + H\mathbf{r}' \cdot (\mathbf{n} + \gamma\mathbf{r}')' + \frac{H^2}{3}|(\mathbf{n} + \gamma\mathbf{r}')'|^2\right). \tag{2.5}$$

Using the basic geometric relations that

$$\mathbf{n}' = -\kappa\mathbf{r}', \mathbf{r}'' = \kappa\mathbf{n},$$

where $\kappa(s)$ is the curvature of the upper surface at s, given by

$$\kappa = \frac{-h''}{\sqrt{1 - (h')^2}}, \tag{2.6}$$

the above formula (2.5) can be reduced to

$$w(h', h'', \gamma, \gamma') = \frac{G}{2}\left[\gamma^2 + H(-\kappa + \gamma') + \frac{H^2}{3}((\gamma' - \kappa)^2 + \gamma^2\kappa^2)\right].$$

We need also consider the gravitational energy of the sheet. By averaging in the corresponding cross section, we could also calculate a reduced formula for gravity as

$$f(h, h', \gamma) = \int_0^H \rho g v(s, y)\,\mathrm{d}y = \rho g\left(h + \frac{H}{2}(\mathbf{n} + \gamma\mathbf{r}') \cdot \mathbf{j}\right)$$

$$= \rho g\left[h + \frac{H}{2}(-\sqrt{1 - (h')^2} + \gamma h')\right].$$

The total free energy density of the thin sheet is the sum of the elastic energy density w and the gravitational one f.

In summary, given the deformation of the upper surface $h(s)$ and the shear function $\gamma(s)$, the reduced energy of a bending elastic sheet in an interval (x_0, x_1) is given by

$$\mathcal{E}(h, \gamma) = \int_{x_0}^{x_1} w(h', h'', \gamma, \gamma') \, ds + \int_{x_0}^{x_1} f(h, h', \gamma) \, ds, \tag{2.7}$$

where

$$w(h', h'', \gamma, \gamma') = \frac{G}{2}\left[\gamma(s)^2 + H(-\kappa + \gamma'(s)) + \frac{H^2}{3}((\gamma'(s) - \kappa)^2 + \gamma(s)^2\kappa^2)\right] \tag{2.8}$$

and

$$f(h, h', \gamma) = \rho g\left[h(s) + \frac{H}{2}(-\sqrt{1 - (h'(s))^2} + \gamma(s)h'(s))\right]. \tag{2.9}$$

Here the curvature κ is given by (2.6).

(b) The stationary problem

With the total energy functional (2.7), we are able to propose an energy minimization problem to study the deformation of a detached region of the thin sheet.

Suppose we are interested in the deformation of the elastic sheet in an interval $s \in (x_0, x_1)$. We set some boundary conditions for $h(s)$ and $\gamma(s)$. On the left boundary $s = x_0$, we set $h(x_0) = H$, $h'(x_0) = 0$, and suppose the shear function $\gamma(s)$ satisfies $\gamma(x_0) = \gamma_0 > 0$. On the right boundary $s = x_1$, we assume that $\gamma(x_1) = 0$ and h satisfies a natural boundary condition. Since the sheet is above the substrate, we also have the constraint that

$$h(s) \geq H.$$

Then we could define the admissible sets for h and γ, respectively.

$$V = \{h \in H^2([x_0, x_1]) \mid h(x_0) = H, h'(x_0) = 0, h(s) \geq H\} \tag{2.10}$$

and

$$W = \{\gamma \in H^1([x_0, x_1]) \mid \gamma(x_0) = \gamma_0, \gamma(x_1) = 0\}. \tag{2.11}$$

With the above boundary conditions, the energy density function can be further simplified. We firstly see that

$$\int_{x_0}^{x_1} \gamma'(s) \, ds = \gamma(x_1) - \gamma(x_0) = -\gamma_0.$$

Denote by θ the angle between τ and the x-axis, then we have

$$\int_{x_0}^{x_1} \kappa(s) \, ds = -\int_{x_0}^{x_1} \theta'(s) \, ds = -\theta(x_1).$$

By the relation that $(\partial_s u, h') = (\cos\theta, \sin\theta)$, we get $\theta = \arcsin(h')$. Thus, we derive that

$$\int_{x_0}^{x_1} \kappa(s) \, ds = -\arcsin h'(x_1).$$

By the above relation, the integration of w can be simplified. The total energy reads

$$\mathcal{E}(h, \gamma) = \tilde{\mathcal{E}}(h, \gamma) - \frac{GH\gamma_0}{2}, \tag{2.12}$$

with

$$\tilde{\mathcal{E}}(h, \gamma) = \int_{x_0}^{x_1} \tilde{w}(h', h'', \gamma, \gamma') \, ds + \int_{x_0}^{x_1} f(h, h', \gamma) \, ds + \frac{GH}{2} \arcsin h'(x_1), \tag{2.13}$$

and

$$\tilde{w}(h', h'', \gamma, \gamma') = \frac{G}{2}\left[\gamma(s)^2 + \frac{H^2}{3}((\gamma' - \kappa)^2 + \gamma^2\kappa^2)\right]. \tag{2.14}$$

Here again the curvature κ is calculated by (2.6). Therefore, the deformation of the elastic gel sheet in the detached region (x_0, x_1) is obtained by minimizing the total elastic energy $\tilde{\mathcal{E}}$. This leads to the following problem:

$$\min_{h \in V, \gamma \in W} \tilde{\mathcal{E}}(h, \gamma).\tag{2.15}$$

3. The Euler–Lagrange equations of the stationary problem

In this section, we perform an asymptotic analysis of the Euler–Lagrange equations of the stationary problem.

(a) A simplified energy

At the moment the study of the full nonlinear energy escapes our capacity, but the analysis of a simplified variant still gives a great insight about the stick–slip mechanism. First, the curvature κ and the square root in the gravitational energy are substituted by

$$\kappa \approx -h''(s), \quad \sqrt{1 - h'^2} \approx 1 - \frac{1}{2}h'^2,\tag{3.1}$$

respectively. In the numerical simulations presented in §6 the derivative h' is indeed relatively small in a large part of the domain, but near the crack tip the approximation does constitute a source of error since there $h'(x) \approx 1$. A second simplification is to consider only functions γ and h such that

$$\gamma'(x_1) = 0, \quad h'(x_1) = 0.\tag{3.2}$$

The energy (2.12) in the detached interval becomes

$$\mathcal{E}(h, \gamma) = \frac{\rho g H}{2}(x_1 - x_0) - \frac{G H \gamma_0}{2} + \int_{x_0}^{x_1} \frac{G}{2}\gamma^2 + \frac{H^2 G}{2 \cdot 3}\left((\gamma' + h'')^2 + \gamma^2 h''^2\right)$$

$$+ \rho g(h - H) + \frac{\rho g H}{2}\left(\frac{1}{2}h'^2 + \gamma h'\right) \mathrm{d}s.\tag{3.3}$$

This energy is considered only in this section: the rest of the paper uses (2.7)–(2.9).

The Euler–Lagrange equations are

$$\frac{H^2 G}{3}\left(h^{(4)} + (\gamma^2 h'')'' + \gamma^{(3)}\right) + \rho g\left(1 - \frac{H}{2}h'' - \frac{H}{2}\gamma'\right) = 0, \quad x \in (x_0, x_1)\tag{3.4}$$

and

$$G\gamma + \frac{H^2 G}{3}\left(-\gamma'' - h^{(3)} + (h'')^2\gamma\right) + \rho g\frac{H}{2}h' = 0.\tag{3.5}$$

We look for solutions to the governing equations such that

$$h(x_0) = H = h(x_1), \quad h'(x_1) = 0 = h'(x_0)\tag{3.6}$$

and

$$\gamma(x_0) = \gamma_0, \quad \gamma(x_1) = 0, \quad \gamma'(x_1) = 0.\tag{3.7}$$

The field γ requires three boundary conditions, which is consistent with the presence of $\gamma^{(3)}$ in the equations. Here we assume that $h(x) > H$ for $x \in (x_0, x_1)$.

(b) An optimality condition for the length of the detached interval

In the wave phenomenon under consideration, the bubble in figure 1 is moving left. One way to understand this is that at a previous infinitesimal instant $t - dt$ the detached interval was $(x_0 + \varepsilon_0, x_1 + \varepsilon_1)$; then the high shear energy accumulated on the left favoured the debonding of the film between $x = x_0$ and $x = x_0 + \varepsilon_0$; then gravity brought the film back in contact with the substrate

6

royalsocietypublishing.org/journal/rspa   *Proc. R. Soc. A* **476:** 20200001

from $x = x_1$ to $x = x_1 + \varepsilon_1$. This may be regarded as a free-boundary problem where the right-end point x_1 is one of the unknowns. We claim that the optimality condition associated with this free-boundary problem is that

$$h''(x_1) = 0. \tag{3.8}$$

In order to justify the claim, suppose that for every ξ between x_1 and $x_1 + \varepsilon_1$ the minimization problem (2.15), with boundary conditions (3.6) and (3.7), defined in the domain (x_0, ξ), has a unique solution that may be denoted by

$$\tilde{h}(x; \xi), \quad \tilde{\gamma}(x; \xi) \quad x \in (x_0, \xi).$$

Then the intuition stated above suggests that $\tilde{h}(\cdot, \xi)$ should be given by

$$\tilde{h}(x; \xi) = \begin{cases} h(x) & x \in [x_0, x_1] \\ H & x \in [x_1, \xi], \end{cases}$$

where $h(x) := \tilde{h}(x; x_1)$ is the solution that is being sought for. Then the total energy

$$\frac{\rho g H}{2}(\xi - x_0) - \frac{G H \gamma_0}{2} + \int_{x_0}^{\xi} \frac{G}{2}\tilde{\gamma}^2 + \frac{H^2 G}{2 \cdot 3}\left((\tilde{\gamma}' + \tilde{h}'')^2 + \tilde{\gamma}^2(\tilde{h}'')^2\right)$$

$$+ \rho g(\tilde{h} - H) + \frac{\rho g H}{2}\left(\frac{1}{2}(\tilde{h}')^2 + \tilde{\gamma}\tilde{h}'\right) ds,$$

is, in principle, given by

$$\frac{\rho g H}{2}(\xi - x_0) - \frac{G H \gamma_0}{2} + \int_{x_0}^{x_1} \frac{G}{2}\gamma^2 + \frac{H^2 G}{2 \cdot 3}\left((\gamma' + h'')^2 + \gamma^2(h'')^2\right)$$

$$+ \rho g(h - H) + \frac{\rho g H}{2}\left(\frac{1}{2}(h')^2 + \gamma h'\right) ds$$

(where γ and h, without tildes, are the solution when $\xi = x_1$). Hence, on the one hand, the expression

$$I(\xi) := \int_{x_0}^{\xi} \frac{G}{2}\tilde{\gamma}^2 + \frac{H^2 G}{2 \cdot 3}\left((\tilde{\gamma}' + \tilde{h}'')^2 + \tilde{\gamma}^2(\tilde{h}'')^2\right) + \rho g(\tilde{h} - H) + \frac{\rho g H}{2}\left(\frac{1}{2}(\tilde{h}')^2 + \tilde{\gamma}\tilde{h}'\right) ds$$

should be constant for $\xi \in (x_1, x_1 + \varepsilon_1)$.

On the other hand, differentiating $I(\xi)$ and letting $\xi \searrow x_1$ gives

$$\left.\frac{dI}{d\xi}\right|_{\xi = x_1} = \frac{H^2 G}{2 \cdot 3} h''(x_1)^2 + \int_{x_0}^{x_1} G\gamma v + \frac{H^2 G}{3}\left((\gamma' + h'')v' + (\gamma' + h'')u'' + (h'')^2\gamma v + \gamma^2 h'' u''\right)$$

$$+ \rho g u + \frac{\rho g H}{2}\left(h'u' + vh' + \gamma u'\right) ds,$$

where

$$u(x) := \left.\frac{\partial \tilde{h}}{\partial \xi}(x; \xi)\right|_{\xi = x_1}, \quad v(x) := \left.\frac{\partial \tilde{\gamma}}{\partial \xi}(x; \xi)\right|_{\xi = x_1}.$$

Applying the chain rule to the boundary conditions

$$\text{for all } \xi \in (x_1, x_1 + \varepsilon_1): \quad \left.\tilde{h}(x; \xi)\right|_{x = \xi} = H, \quad \left.\frac{d\tilde{h}}{dx}(x; \xi)\right|_{x = x_1} = 0,$$

and the analogous condition for γ, we find that

$$\left.\frac{d\tilde{h}}{dx}(x; \xi)\right|_{\substack{x = x_1 \\ \xi = x_1}} + u(x_1) = 0 \quad \text{and} \quad h''(x_1) + u'(x_1) = 0.$$

Table 1. The values of the density and elastic modulus are standard amounts for Polyethylene. The actual aspect ratio of the membrane, taken from data in [18,19] is $5/150$, smaller than β, but of the same order of magnitude. The range of values for ℓ is that exhibited in the simulations of §6. The gravitational acceleration $g = 9.8$ in the definition of ζ is measured in m · s^{-2}.

elastic modulus	G (Pa)	0.1×10^6
dimensionless length of detached interval	$l = x_1 - x_0 (m)$	0.08–0.25
dimensionless height of the membrane	$H(m)$	0.01
density	$\rho \left(\frac{kg}{m^3} \right)$	10^3
aspect ratio	$\beta = \frac{H}{l}$	0.125–0.04
gravity to elasticity ratio	$\zeta = \sqrt{\frac{3\rho g}{2HG}}\,\ell$	0.31–0.96

8

royalsocietypublishing.org/journal/rspa   *Proc. R. Soc. A* **476**: 20200001

Integrating by parts and using these expressions, together with the Euler–Lagrange equations, it follows that:

$$\frac{dI}{d\xi}\bigg|_{\xi=x_1} = \frac{H^2 G}{2\cdot 3} h''(x_1)^2 + \frac{H^2 G}{3}\left((\gamma' + h'')u' + \gamma^2 h'' u'\right)\bigg|_{x=x_1} = -\frac{H^2 G}{2\cdot 3} h''(x_1)^2.$$

By virtue of the above calculation, the condition $h''(x_1) = 0$ admits the interpretation of the absence of configurational forces that would make the bubble unstable and favour it to slide rightwards, attaining lower energy states.

(c) Dimensionless form of the equations

Table 1 summarizes the geometric and physical parameters of the problem. We introduce the dimensionless variables and fields

$$\bar{x} = \frac{x - x_0}{l}, \quad \bar{s} = \frac{s}{l}, \quad \bar{\gamma}(\bar{x}) = \gamma(x), \quad \bar{h}(\bar{x}) = \frac{h(x)}{H} \geq 1, \quad \bar{s}, \bar{x} \in [0,1]. \tag{3.9}$$

For notational convenience, we keep the symbol $'$ to still denote $d/d\bar{x}$, and drop the superimposed bar in the dependent variables. We rewrite equation (3.4) in terms of the new dimensionless variables and multiply through by $3\ell^4/(H^3 G)$. This yields

$$\beta^2 h^{(4)} + \beta^2 (\gamma^2 h'')'' - \zeta^2 \beta^2 h'' + \beta \gamma^{(3)} - \zeta^2 \beta \gamma' = -2\zeta^2, \quad \bar{x} \in (0,1). \tag{3.10}$$

The same scaling approach and notational convention applied to equation (3.5) gives

$$\gamma - \frac{\beta^2}{3}\gamma'' - \frac{\beta^3}{3}h^{(3)} - \frac{\beta^4}{3}(h'')^2\gamma + \frac{\zeta^2}{3}\beta^3 h' = 0, \quad \bar{x} \in (0,1). \tag{3.11}$$

We now look for approximate solutions of the system satisfying the boundary conditions

$$\gamma(0) = \gamma_0, \quad \gamma(1) = 0, \quad \gamma'(1) = 0 \tag{3.12}$$

and

$$h(0) = 1 = h(1), \quad h'(0) = 0 = h'(1), \tag{3.13}$$

and such that $h(x) > 1$.

(d) Asymptotic analysis

The terms with h in the system (3.10) and (3.11) would be well balanced with the terms involving γ if the magnitude of the derivatives of h were comparable to the large quantity β^{-2} and γ and its derivatives were of order β. That a γ of order β cannot match the boundary condition $\gamma(0) = \gamma_0$, is indicative of a boundary layer for $\gamma(x)$. This is consistent with the finite-element solution of §6 and expresses that the unsustainable shear is relieved very rapidly, transforming in a very

short interval the accumulated shear energy into bending and gravitational energies. The terms $\gamma - (\beta^2/3)\gamma''$ are reminiscent of the Allen–Cahn equation for phase transitions, as well as the classical Prandtl's equations in fluid mechanics. It thus seems reasonable to look for solutions admitting the asymptotic expansion:

$$\gamma(\bar{x}) = \Gamma_0\left(\frac{\sqrt{3}}{\beta}\bar{x}\right) + O(\beta) \tag{3.14}$$

and

$$h(\bar{x}) = \Xi_0\left(\frac{\sqrt{3}}{\beta}\bar{x}\right) + \beta^{-2}h_0(\bar{x}) + O(\beta^{-1}). \tag{3.15}$$

One of the implications is that the transition for γ occurs in an interval of width comparable to the film thickness. A heuristic understanding of this is the following. If γ decays from γ_0 to 0 in a distance η then $\gamma' \approx \gamma_0/\eta$. The bending energy in (3.3) is reduced when $\kappa \approx \gamma'/(1 + \gamma^2)$. This negative curvature bends the film upwards, separating it from the substrate. The bending energy in that transition interval is, hence, of order $\eta \cdot H^2 G \cdot \gamma'^2 \approx \eta \cdot G\gamma_0^2 \cdot (H/\eta)^2$, whereas the shear energy is of order $\eta \cdot G\gamma_0^2$. If it takes too long to realign the top and the bottom layers then a large shear energy is paid (and $G \approx 10^5$ Pa, so no mistakes are allowed). If γ drops too rapidly, then the bending energy is prohibitive. This results in an equipartition of energy where the transition length is of order $\eta \approx H$, which in the dimensionless variable $\bar{x} = x/\ell$ corresponds to a width of order $H/l \approx \beta$.

(e) Exchange between the bending and gravitational energies

The above considerations, together with the finite-element results of §6, show that in most of the interval (x_0, x_1) the shear function γ is very small and the governing equation for h is essentially

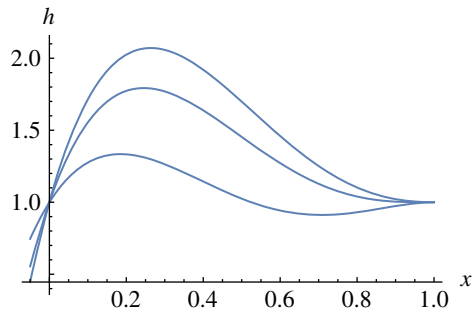$$h^{(4)}(\bar{x}) - \zeta^2 h''(\bar{x}) = -2\zeta^2\beta^{-2}, \quad \bar{x} \in (0, 1). \tag{3.16}$$

The general solution of this linear fourth-order equation is

$$h(\bar{x}) = A + B\bar{x} + C e^{-\zeta x} + D e^{\zeta x} + \beta^{-2}x^2. \tag{3.17}$$

The boundary condition $h'(0) = 0$ is not meaningful because it is quickly subsumed by the boundary layer term $\Xi_0(\sqrt{3}\bar{x}/\beta)$ for h. (Due to the absorption of the shear energy, h begins with a convex profile, but gravity rapidly turns it into a concave one. What happens in the short transition interval for γ, and how it fuels the bending upwards of the film, is not seen by the equation just presented, which is valid in the region where γ has essentially vanished.) But the remaining boundary conditions:

$$h(0) = 0, \quad h(1) = 1, \quad h'(1) = 0, \tag{3.18}$$

are meaningful and reduce the intricate nonlinear PDE system to the problem of just choosing between a one-parameter family of curves. One possibility is to write down the solution depending of the value of h' at $\bar{x} = 0$ (which can in turn be regarded as a measure of the shear energy coming from the attached portion of the film on the left). What is observed is the following. For a given fixed interval length ℓ, if $h'(0)$ is relatively small, then the film initially lifts upwards but then gravity brings h back to $h(\bar{x}) = 1$ at a point $\bar{x}$ to the left of the right-end of the interval $\bar{x} = 1$. This is consistent with the intuition that a small shear energy cannot sustain too much gravitational energy so the film drops back in contact with the substrate very rapidly. If, on the contrary, $h'(0)$ is too large, then the larger its value, the taller the profile curve for h. This corresponds to a film that is clamped at $x = x_1$ and buckles more and more upwards because it receives too much energy from the left. It would prefer to slide to the right were it not for the boundary condition $h(x_1) = H$ (in the original variables). Finally, the smallest positive value of $h'(0)$ that produces a solution $h(\bar{x})$ satisfying $h > 1$ in all of the interval $\bar{x} \in (0, 1)$, is precisely the unique value of $h'(0)$ for which the solution satisfies the optimality condition $h''(1) = 0$ for the free-boundary problem (3.8). Figure 3 is representative of this behaviour. Figure 4 shows the unique

9

royalsocietypublishing.org/journal/rspa   Proc. R. Soc. A **476**: 20200001

10

royalsocietypublishing.org/journal/rspa   Proc. R. Soc. A **476**: 20200001

Figure 3. Solutions of (3.16), with fixed $\ell = 0.16$, for various values of $h'(0)$. When $h'(0) = 4.2$, the film fails to be above the moving substrate. When $h'(0) = 7.7$ the optimality condition $h''(0) = 0$ is satisfied. When $h'(0) = 9.6$ the solution overestimates the true profile of h. (Online version in colour.)
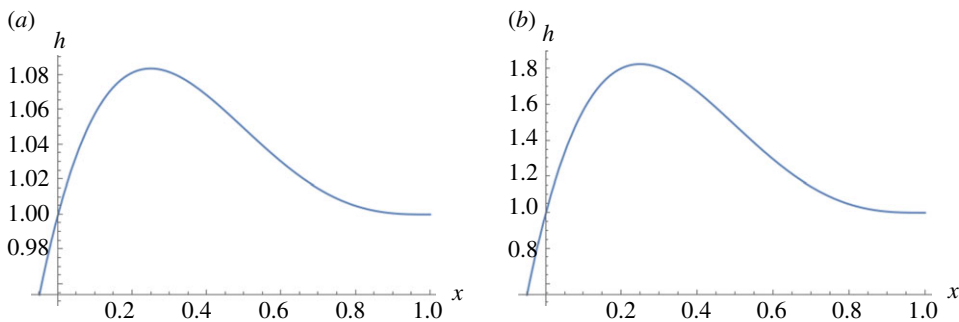
Figure 4. Optimal solutions of (3.16) for various values of ℓ. (a) $\ell = 0.09$, the optimality condition $h''(1) = 0$ being satisfied only when $h'(0) = 0.796$. The maximum height is 1.08. (b) $\ell = 0.16$, $h'(0) = 7.912$, and the maximum height is 1.83. (Online version in colour.)

profile associated with ℓ, for two values of ℓ. The solutions are in very good qualitative agreement with the finite-element simulations of §6 for the coupled nonlinear system. In particular, even if the derivatives of h are large (which is consistent with the asymptotic analysis that suggests that they are of order β^{-2}), the values of h itself remain comparable to the film thickness (in the range from 1 to 3 cm when the film is 1 cm thick and ℓ is between 8 and 20 cm, and a maximum height of 6 cm for ℓ of 25 cm).

(f) Boundary layer

The question remains as to how does the length ℓ of the detached interval (and, hence, the maximum height above the substrate and the whole profile of h) depend on the shear threshold γ_0. Plugging expansions (3.14) and (3.15) into equations (3.10) and (3.11), then keeping only the leading-order terms, yields a nonlinear system coupling the boundary layer term Γ_0 for γ with the term Ξ_0 for h. Solving such a complicated system goes beyond the scope of this article. Here we limit ourselves to presenting a simple ansatz that gives a sense of how the shear boundary condition $\gamma(x_0) = \gamma_0$ is transmitted so that h obtains the missing degree of freedom in order to be completely determined.

The idea is to explore what would happen if $\gamma(\bar{x})$ were given by the solution

$$\gamma(\bar{x}) = \gamma_0 \, e^{-(\sqrt{3}/\beta)\bar{x}}$$
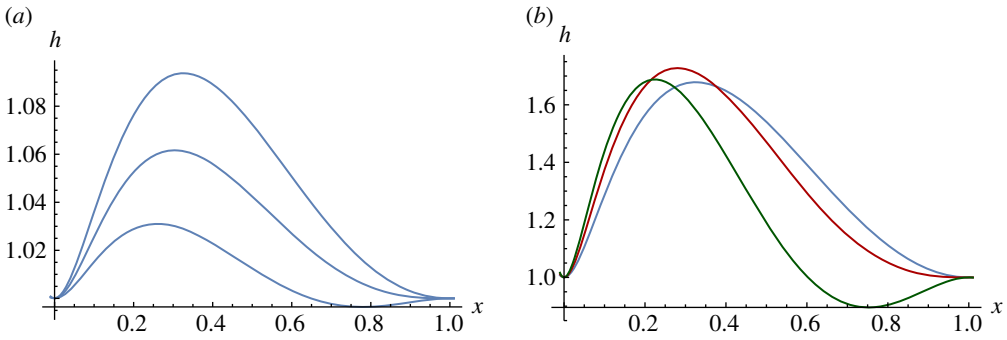
Figure 5. Optimal solutions of (3.10) with the approximation $\gamma(x) = \gamma_0 e^{-(\sqrt{3}/\beta)\bar{x}}$, for different values of γ_0. (a) When $\ell = 0.09$, the only γ_0 for which the curve satisfies the free-boundary optimality criterion $h''(1) = 0$ is approximately $\gamma_0 = 0.037$. The plot also shows the curves obtained for the same ℓ but with $\gamma_0 = 0.025$ (below) and $\gamma_0 = 0.049$ (above). The plot on (b) shows that when $\gamma_0 = 0.19$ then the film takes a distance of $\ell = 0.16$ to fall down again (middle curve, in red). If ℓ were only $\ell = 0.13$ (right-most curve, in blue) then $h''(1) > 0$ and the film prefers to slide further to the right. If $\ell = 0.19$ (curve below, in green) then γ_0 is not big enough to sustain the large gravitational energy required to prevent it from falling at exactly that distance. (Online version in colour.)

to the boundary value problem

$$\gamma - \frac{\beta^2}{3}\gamma'' \equiv 0, \quad \gamma(0) = \gamma_0,$$

together with the requirement that $\Gamma_0(\tilde{x})$ decays exponentially as $\tilde{x} = (\sqrt{3}/\beta)\bar{x}$ goes to infinity. Substituting in (3.10) and ignoring the cubic term $(\gamma^2 h'')'$, we obtain the general solution

$$h(\bar{x}) = A + B\bar{x} + C e^{-\zeta x} + D e^{\zeta x} + \beta^{-2} x^2 + \frac{1}{\sqrt{3}} \cdot \frac{1 + \frac{1}{3}\zeta^2\beta^2}{3 - \zeta^2\beta^2} \gamma_0 e^{-(\sqrt{3}/\beta)\bar{x}}. \tag{3.19}$$

As shown in figure 5, the optimal distance ℓ at which the film falls back in contact with the moving plate is the only ℓ for which the boundary conditions (3.18), the condition $h'(0) = 0$ and the optimality criterion (3.8), regarded as a system in the unknowns A, B, C, D and ℓ, has a solution.

4. A dynamic model using Onsager Principle

As shown in figure 1, suppose we fix the left boundary of the thin gel sheet and move the substrate in the right direction. Due to the adhesion force, no slippage is allowed between the sheet and the substrate. Initially, the sheet keeps attached with the bottom surface and the shear stress increases in the sheet. Then the pure shear state cannot be sustained by the adhesive force and detachment of the sheet will occur. The detached regions move to the left like a wave. This process will release energies. We now develop a dynamic model for the sliding gel sheet problem.

When the gel sheet slides on a substrate, there generally exist a few attached regions and detached regions as shown in figure 1. Denote by L the length of the sheet. At time t, we suppose that the attached regions in the reference domain are given by

$$\mathcal{A} = \{(x_0, x_1), (x_2, x_3), \ldots, (x_{2i}, x_{2i+1}), \ldots\},$$

and the detached regions are given by

$$\mathcal{D} = \{(x_1, x_2), (x_3, x_4), \ldots, (x_{2i+1}, x_{2i+2}), \ldots\}.$$

Here $x_0 = 0$ and $x_N = L$ corresponds to the end points of the sheet. We assume that $(x_0, x_1) \in \mathcal{A}$. However, (x_{N-1}, x_N) can either be an attached region or a detached region. Except the two points $x_0 = 0$ and $x_N = L$, all other points change positions with time so that

$$x_i = x_i(t), \quad 1 < i < N - 1.$$

The number N is also unknown. Initially, we set $N = 1$, implying that the whole sheet is attached to the substrate at $t = 0$.

The energy in the detached regions could be described by the model given in the previous section. In the attached regions, only the shear stress contributes to the elastic energy. The energy density in the attached regions is simply

$$\frac{G}{2}\gamma^2(s) + \frac{\rho g H}{2}.$$

Therefore, the total energy of the sheet is given by

$$\mathcal{E}(h, \gamma, t) = \sum_{I_i \in \mathcal{D}} \int_{I_i} w(h', h'', \gamma, \gamma'') + f(h, h', \gamma)\, ds + \sum_{I_i \in \mathcal{A}} \int_{I_i} \frac{G}{2}(\gamma(s))^2 + \frac{\rho g H}{2}\, ds. \tag{4.1}$$

Here we denote $I_i = (x_i, x_{i+1})$. Similar to the derivation in §2b, the energy could be rewritten as

$$\mathcal{E}(h, \gamma, t) = \sum_{I_i \in \mathcal{D}} \left[\int_{I_i} \tilde{w}(h', h'', \gamma, \gamma') + \tilde{f}(h, h', \gamma)\, ds - \frac{GH\gamma_0}{2} \right] + \frac{G}{2} \sum_{I_i \in \mathcal{A}} \int_{I_i} (\gamma(s))^2\, ds$$

$$+ \frac{GH}{2} \arcsin h'(x_N) + \frac{\rho g H L}{2}, \tag{4.2}$$

with $\tilde{f}(h, h', \gamma) = \rho g(h + (H/2)(-1 - \sqrt{1 - (h')^2} + \gamma h'))$ and $\tilde{w}$ is given in (2.14). Here γ_0 is the left boundary condition for γ in an detached region. The existence of the terms $-GH\gamma_0/2$ and $\rho g H L/2$ do not affect the solution of an energy minimization problem. For simplicity in notations, we will ignore them in following discussions.

On the attached region, the shear function $\gamma(t)$ satisfies that

$$H\frac{d\gamma}{dt} = v_{\text{wall}}, \tag{4.3}$$

where v_{wall} is the wall velocity. The ordinary differential equation needs to be solved for a point when it attaches the substrate from a detached state with an initial condition $\gamma = 0$. Since the first-attach time might be different for the points in an attached region, $\gamma(x, t)$ is a function of both position and time.

Suppose that we are not interested in the fast dynamical process of how a detached region approaches its equilibrium state. In the detached regions, the shape of the thin sheet is determined by minimizing the total energy given the boundary conditions for γ and h. The boundary condition of γ can be obtained by solving the ordinary boundary equation (4.3) in neighbouring attached regions. More precisely, for each interval $I_{2i-1} = (x_{2i-1}, x_{2i}) \in \mathcal{D}$, $2i < N$(the detached region not at the right end), the deformation of the region is given by minimizing the total energy

$$\mathcal{E}_{I_{2i-1}}(h, \gamma) = \int_{I_{2i-1}} \tilde{w}(h', h'', \gamma, \gamma') + \tilde{f}(h, h', \gamma)\, ds,$$

under the boundary conditions that

$$h(x_{2i-1}) = H, h'(x_{2i-1}) = 0, \gamma(x_{2i-1}) = \gamma|_{I_{2i-2}}(x_{2i-1}) \tag{4.4}$$

and

$$h(x_{2i}) = H, h'(x_{2i}) = 0, \gamma(x_{2i}) = 0.$$

Notice that the boundary condition on x_{2i} is slightly different from that described in last section (when the point is the right end of the sheet), where a natural boundary condition is used. We assume there is no shear at the right attached point($\gamma(x_{2i}) = 0$) since the asymptotic analysis in §3

shows that the shear in the detached region decays exponentially. When $2i = N$, i.e. $(x_{N-1}, x_N) \in \mathcal{D}$, the deformation of the region is given by minimizing the energy

$$\mathcal{E}_{I_{N-1}}(h, \gamma) = \int_{I_{N-1}} \tilde{w}(h', h'', \gamma, \gamma') + \tilde{f}(h, h', \gamma) \, ds + \frac{GH}{2} \arcsin h'(x_N),$$

under a boundary condition similar to (4.4) for x_{N-1} and a natural boundary condition for the right endpoint x_N.

Given the position of a detached region and the boundary conditions, we solve the above energy minimization problem and obtain a minimizer $(\tilde{h}, \tilde{\gamma})$. This can be done for all the detached regions. Then, the total energy in the thin sheet is reduced to

$$\mathcal{E}_r(x_1(t), \ldots, x_N(t)) = \sum_{I_i \in \mathcal{D}} \int_{I_i} w(\tilde{h}', \tilde{h}'', \tilde{\gamma}, \tilde{\gamma}') + \tilde{f}(\tilde{h}, \tilde{h}', \tilde{\gamma}) \, ds + \frac{G}{2} \sum_{I_i \in \mathcal{A}} \int_{I_i} (\gamma(s))^2 \, ds$$

$$+ \frac{GH}{2} \arcsin \tilde{h}'(x_N). \tag{4.5}$$

Now we develop a model for the dynamics of $x_i(t)$, the points separating the attached regions and the detached regions. For that purpose, we use the Onsager principle [20–23]. When the sheet detaches from the substrate, some energy will be dissipated. In general, the energy dissipation function, which is defined as half of the total energy dissipation rate of the sheet, is given by

$$\Phi(\dot{x}_1, \ldots, \dot{x}_N) = \frac{\xi}{2} \sum_{i=1}^{N} (\dot{x}_i^+)^\alpha. \tag{4.6}$$

Here ξ and α are two positive phenomenological parameters depending on the material property of the gel and the substrate [18]. $\dot{x}_i^+$ denotes the moving velocity of x_i in the outer direction of $\mathcal{D}$, i.e.

$$\dot{x}_i^+ = \begin{cases} |\dot{x}_i|, & \text{if } \dot{x}_i < 0 \text{ for odd } i \text{ or } \dot{x}_i > 0 \text{ for even } i, \\ 0, & \text{otherwise.} \end{cases} \tag{4.7}$$

This implies that only the detaching process dissipates the energy while the re-attaching does not. Physically, the dissipation in the detachment is due to the adhesive debonding between the gel film and the substrate [24]. In the following, we choose $\alpha = 2$ for simplicity.

Denote the Rayleighian as the sum of the energy dissipation function and the decreasing rate of the total potential energy in the system

$$\mathcal{R}(\dot{x}_1, \ldots, \dot{x}_N) = \Phi(\dot{x}_1, \ldots, \dot{x}_N) + \frac{d\mathcal{E}_r(\dot{x}_1, \ldots, \dot{x}_N)}{dt} = \Phi(\dot{x}_1, \ldots, \dot{x}_N) + \sum_{i=1}^{N} \frac{d\mathcal{E}_r}{dx_i} \dot{x}_i.$$

Then the dynamic of x_i is obtained by minimizing the Rayleighian with respect to $\dot{x}_1, \ldots, \dot{x}_N$. The calculations for $d\mathcal{E}_r/dx_i$ are quite complicated since the solution of the energy minimization problem in the detached region may also depend on the position of x_i. For example, for odd i, we need to calculate

$$\frac{d\mathcal{E}_r}{dx_i} = \frac{\partial}{\partial x_i} \left(\int_{x_{i-1}}^{x_i} \frac{G}{2} \gamma^2 \, ds \right) + \frac{\partial}{\partial x_i} \left(\int_{x_i}^{x_{i+1}} w(\tilde{h}', \tilde{h}'', \tilde{\gamma}, \tilde{\gamma}') + \tilde{f}(\tilde{h}, \tilde{h}', \tilde{\gamma}) \, ds \right). \tag{4.8}$$

The calculations for the second term are complicated since $(\tilde{h}, \tilde{\gamma})$ also depends on the x_i. The calculations can be simplified under the assumption that the first term in (4.8) is much larger than the second term. The assumption is reasonable from the physical point of view. Firstly, the average energy density in a detached region (x_i, x_{i+1}) is much smaller than $(G/2)(\tilde{\gamma}(x_i))^2$. That is

why the detachment occurs. Secondly, experiments show that the detached region (x_i, x_{i+1}) moves in a wavelike way. The total energy in this region does not change much with the motion of x_i. Therefore, we can calculate the generalized force in an approximation that

$$\mathcal{F}(x_i) = \frac{\mathrm{d}\mathcal{E}_r}{\mathrm{d}x_i} \approx \frac{\partial}{\partial x_i}\left(\int_{x_{i-1}}^{x_i} \frac{G}{2}\gamma^2\,\mathrm{d}s\right) = \frac{G}{2}(\gamma(x_i)|_{I_{i-1}})^2 = \frac{G}{2}(\tilde{\gamma}(x_i)|_{I_i})^2, \tag{4.9}$$

for odd i. The approximation is exact when i is equal to N.

For x_i with odd i, i.e. the left point of a detached region, by the Onsager principle

$$\frac{\delta\Phi}{\delta\dot{x}_i} + \mathcal{F}(x_i) = 0,$$

we have

$$\xi\dot{x}_i = -\max\left(\mathcal{F}(x_i),\,0\right) = -\frac{G}{2}(\gamma(x_i)|_{I_{i-1}})^2. \tag{4.10}$$

This implies that x_i moves left whenever $\gamma(x_i)|_{I_{i-1}} \neq 0$. This is not consistent with experimental observations. In reality, there is always an energy barrier that blocks the detachment which has not been considered in above derivation. To consider the energy barrier, we assume that the detachment happens when the force $\mathcal{F}(x_i)$ is larger than a critical value $\sigma > 0$. This leads to the following modified dynamics:

$$\xi\frac{\mathrm{d}x_i}{\mathrm{d}t} = -\max\left(\frac{G}{2}(\tilde{\gamma}(x_i)|_{I_i})^2 - \sigma, 0\right), \tag{4.11}$$

for the detaching point x_i when i is odd. Specifically, if i is odd and equal to N, which implies $I_{N-1} = (x_{N-1}, x_N)$ is an attached region, detachment occurs at x_N when $(G/2)(\gamma(x_N)|_{I_{N-1}})^2$ is larger than σ.

Similar calculations can be done for the right point of a detached region (for even i). Due to the boundary condition $\gamma(x_i) = 0$ for the right point, the generalized force $\mathcal{F}(x_i) \approx 0$. We assume that the force is always smaller than the critical value σ.

Therefore, by a similar derivation as above, the right point of a detached region does not move outwards

$$\frac{\mathrm{d}x_i}{\mathrm{d}t} = 0, \quad \text{for even } i. \tag{4.12}$$

Nevertheless, the right detached point may change positions when we minimize the energy functional $\mathcal{E}_{i-1}$ in the detached region I_{i-1}. The minimizer may correspond to a smaller detached region and part of I_{i-1} in the right end actually attaches to the substrate. This implies the point x_i can move inwards. This will be shown in numerical experiments in §5.

5. Numerical methods

(a) A gradient flow method for the stationary problem

We first develop a numerical method for the stationary problem to minimize the reduced energy defined in (4.2) in an interval $I_i = (x_i, x_{i+1})$ for odd i. Here we have two unknown functions γ and h. We would like to solve the problem by the alternating direction method, which is widely used in optimization with multiple variables. The method is quite simple and easy to implement. Basically, it is an iterative method. The main steps are as follows. For given h^{k-1} and γ^{k-1} in $(k-1)$th step, we compute two sub-problems alternatively

    — Solve Problem (P_1): $h^k = \operatorname{argmin}\mathcal{E}_{I_i}(h, \gamma^{k-1})$;
    — Solve Problem (P_2): $\gamma^k = \operatorname{argmin}\mathcal{E}_{I_i}(h^k, \gamma)$.

The two sub-problems can be solved by gradient flow methods. Notice that the corresponding Euler–Lagrange equations are a fourth-order partial differential equation for h and a second-order one for γ. This motivates us to consider different gradient flows for h and γ.

14

royalsocietypublishing.org/journal/rspa Proc. R. Soc. A 476: 20200001

Problem (P_1) is difficult since its Euler–Lagrange equation corresponds to a fourth-order partial differential equation. Standard gradient flow equation in L^2 will lead to serious restrictions on the time step δt. Therefore, we need to consider a more elaborate gradient flow method to solve this problem. Here we choose a H^2-gradient flow defined as follows:

$$\int_{x_i}^{x_{i+1}} \partial_{ss}\dot{h}\partial_{ss}v = -\left\langle \frac{\delta\mathcal{E}_{I_i}(h,\gamma^{k-1})}{\delta h}, v \right\rangle, \tag{5.1}$$

where $\dot{h} = \partial_t h$ and v is a test function in H^2. This is a time-dependent problem and the total energy decays with increasing time.

We first discretize the problem (5.1) in time. Suppose $h^k(s,t)$ is the solution of (5.1). Let $\delta t > 0$ be the time step length and denote $h^{k,l}(s) \approx h^k(s,l\delta t)$. Discretize the time derivative by the standard finite difference $\dot{h}^k \approx (h^{k,l} - h^{k,l-1})/\delta t$. We obtain

$$\int_{x_i}^{x_{i+1}} \partial_{ss}\left(\frac{h^{k,l} - h^{k,l-1}}{\delta t}\right)\partial_{ss}v\,ds = -\left\langle \frac{\delta\mathcal{E}_{I_i}(h^{k,l},\gamma^{k-1})}{\delta h}, v \right\rangle. \tag{5.2}$$

The variation problem corresponds to a nonlinear partial differential equation, which is the Euler–Lagrange equation of the following energy minimizing problem:

$$\frac{\delta t}{2}\int_{x_0}^{x_1}\left(\partial_{ss}\left(\frac{h - h^{k,l-1}}{\delta t}\right)\right)^2 dx + \mathcal{E}_{I_i}(h,\gamma^{k-1}) - \mathcal{E}_{I_i}(h^{k,l-1},\gamma^{k-1}). \tag{5.3}$$

We linearize the second term of (5.3) and approximate the solution by

$$h^{k,l} = \operatorname{argmin}\frac{\delta t}{2}\int_{x_0}^{x_1}\left(\partial_{ss}\left(\frac{h - h^{k,l-1}}{\delta t}\right)\right)^2 dx + \left\langle \frac{\delta\mathcal{E}_{I_i}}{\delta h}(h^{k,l-1},\gamma^{k-1}), h - h^{k,l-1} \right\rangle. \tag{5.4}$$

The energy minimizing problem in (5.4) corresponds to a linear Euler–Lagrange equation for h and can be solved easily. In real simulations, we do not need to solve problem (P_1) for infinitely long time. Instead, we solve the equation (5.4) until l is equal to a given positive large number l_0 and assume that the solution $h^k(s)$ of (P_1) is approximated by $h^{k,l_0}(s)$.

We then consider the spatial discretization of the problem. We use the finite difference method. Consider a uniform partition of (x_i, x_{i+1}) that $x_i = s_0 < s_1 < \cdots < s_M = x_{i+1}$, with $\Delta s = s_j - s_{j-1}$ for $j = 1,\dots,M$. Let γ_j and h_j be approximations of $\gamma(s_j)$ and $h(s_j)$ for $j = 0,\dots,M$. For simplicity, we ignore the upper labels (k,l) in γ and h. Standard finite difference discretizations lead to

$$\partial_s\gamma(s_j) \approx \frac{\gamma_{j+1} - \gamma_{j-1}}{2\Delta s} + O(\Delta s^2),$$

$$\partial_s h(s_j) \approx \frac{h_{j+1} - h_{j-1}}{2\Delta s} + O(\Delta s^2)$$

and

$$\partial_{ss}h(s_j) \approx \frac{h_{j+1} - 2h_j + h_{j-1}}{\Delta s^2} + O(\Delta s^2).$$

Then $\kappa(s_j), j = 1,\dots,N$, can be approximated by

$$\kappa_j \approx -\frac{h_{j+1} - 2h_j + h_{j-1}}{\Delta s^2(1 - (h_{j+1} - h_{j-1})^2/\Delta s^2)^{1/2}}. \tag{5.5}$$

Then the energy densities at s_j can be approximated by

$$\tilde{w}_j = \frac{G}{2}\left[\gamma_j^2 + \frac{H^2}{3}\left(\left(\frac{\gamma_{j+1} - \gamma_{j-1}}{2\Delta s} - \kappa_j\right)^2 + \gamma_j^2\kappa_j^2\right)\right] \tag{5.6}$$

and

$$\tilde{f}_j = \rho g\left[h_j + \frac{H}{2}\left(-1 + \gamma_j\frac{h_{j+1} - h_{j-1}}{2\Delta s} - \sqrt{1 - (\frac{h_{j+1} - h_{j-1}}{2\Delta s})^2}\right)\right], \tag{5.7}$$

where $j = 1, \ldots M - 1$. For $j = 0$ and M, we use the boundary conditions to approximate the corresponding variables. At the left boundary $j = 0$, using the condition $h'(s_0) = 0$, we can introduce a $h_{-1} = h_1$. Notice also $h(s_0) = H$, then we have

$$\kappa_0 = \frac{2(h_0 - h_1)}{\Delta s^2},$$

$$\tilde{f}_0 = \rho g \left(H + \frac{H}{2}(-1 + 0 - 1) \right) = 0$$

and

$$\tilde{w}_0 = \frac{G}{2} \left[\gamma_0^2 + \frac{H^2}{3} \left(\left(\frac{\gamma_1 - \gamma_0}{\Delta s} - \kappa_0 \right)^2 + \gamma_0^2 \kappa_0^2 \right) \right].$$

Similarly for $j = M$, we have

$$\kappa_M = \frac{2(h_M - h_{M-1})}{\Delta s^2},$$

$$\tilde{f}_M = \frac{\rho g(h_M - H)}{2}$$

and

$$\tilde{w}_M = \frac{G}{2} \left[\gamma_M^2 + \frac{H^2}{3} \left(\left(\frac{\gamma_M - \gamma_{M-1}}{\Delta s} - \kappa_M \right)^2 + \gamma_M^2 \kappa_M^2 \right) \right].$$

With these notations, the discrete energy is written as

$$\mathcal{E}_{h,I_i}(\mathbf{h}, \mathbf{g}) = \frac{\tilde{w}_0 + \tilde{w}_M}{2} \Delta s + \sum_{i=1}^{M-1} \tilde{w}_i \Delta s + \frac{\tilde{f}_M}{2} \Delta s + \sum_{i=1}^{M-1} \tilde{f}_i \Delta s, \tag{5.8}$$

where $\mathbf{h} = (h_1, \ldots h_M)^T$ and $\mathbf{g} = (\gamma_1, \ldots, \gamma_{M-1})^T$.

We discretize the problem (5.4) using the above formula. This leads to an algebraic system for $\mathbf{h}^{k,l}$ in every time step. We solve the algebraic equation for $l = 1, \ldots l_0$ and obtain the solution for Problem (P_1).

For Problem (P_2), we solve it by a simple gradient descent approach as below.

— Give a positive integer l_1 and tolerance $TOL > 0$, set $\mathbf{g}^{k,0} = \mathbf{g}^{k-1}$;
— Compute the derivatives $(\partial \mathcal{E}_{h,I_i} / \partial \gamma_i)(\mathbf{h}^k, \mathbf{g}^{k,l-1})$;
— Set $\mathbf{g}^{k,l} = \mathbf{g}^{k,l-1} + \tau(\partial \mathcal{E}_{h,I_i} / \partial \gamma_i)(\mathbf{h}^k, \mathbf{g}^{k,l-1})$; If $l < l_1$ or $\|\mathbf{g}^{k,l} - \mathbf{g}^{k,l-1}\| \leq TOL$, go back to the last step;
— Set $\mathbf{g}^k = \mathbf{g}^{k,l}$.

Here $\tau > 0$ is a small positive number to make sure the discrete energy decays in each step. The gradient descent method is actually a discrete version of the standard L^2 gradient flow method.

(b) A numerical scheme for the dynamic problem

Based on the numerical solution of the energy minimizing problem in detached regions, we develop a numerical scheme for the dynamic problem described in §4. We aim to compute the evolution of the configuration of the thin gel sheet with respect to time. The evolution of the points between the detached regions and the attached regions are continuous in time. We will discretize the dynamic process. For that purpose, we choose time steps

$$0 = t_0 < t_1 < t_2 < \cdots,$$

where $\Delta t = t_{n+1} - t_n$ is a small time step size.

Initially (when $t = t_0$), the sheet attaches to the substrate completely with no deformation. The attached region set is $\mathcal{A} = \{(x_0(t_0), x_1(t_0))\}$ with $x_0(t_0) = 0$ and $x_1(t_0) = L$. The detached region set is empty, i.e. $\mathcal{D} = \emptyset$. We set $\gamma(s, t_0) = 0$ in the attached region (x_0, x_1).

At time t_n the configuration of the thin sheet is composed by the detached regions in $\mathcal{D}$ and the attached regions in $\mathcal{A}$. In the attached regions, the deformation of the sheet is characterized by a

shear stress $\gamma(s, t_n)$. In the detached regions, the deformation of the sheet is given by $\tilde{h}(s, t_n)$ and $\tilde{\gamma}(s, t_n)$. (These functions may have been discretized in space.) We will compute the configuration changes at next time step t_{n+1} by the following scheme.

— (**Compute the shear function in attached region**.) Solve equation (4.3) in every interval $I_i^n = (x_i(t_n), x_{i+1}(t_n))$ in $\mathcal{A}$ (for even i) numerically:

$$\gamma^{n+1}(s) = \gamma^n(s) + \frac{\Delta t v_{\text{wall}}}{H}, \quad \text{for } s \in I_i.$$

— (**Compute the motion of the left attached point**.) In every detached region I_i^n in $\mathcal{D}$ (for odd i), we compute the motion of the left detached point $x_i(t_n)$ by solving the ordinary differential equation (4.11) to get $x_i(t_{n+1})$.

— (**Check if an attached region arrives at the left end**.) If $x_1(t_{n+1}) \leq x_0 \equiv 0$, the detached point x_1 reaches the left end x_0. We assume the detached region (x_0, x_2) re-attached with the substrate with zero shear stress. Thus, we set $\gamma^{n+1}(s) = 0$ and $h(s) = H$ in (x_0, x_2). We then eliminate the points x_1 and x_2. We set $x_i = x_{i+2}$ for $i = 1, \ldots, N-2$. Then set $N = N - 2$. In the process, the numbers of intervals decreases by 1 in both $\mathcal{A}$ and $\mathcal{D}$.

— (**Check if detachment occurs on the right end**.) If $I_{N-1}^n = (x_{N-1}(t_n), x_N(t_n))$ is an attached region (in $\mathcal{A}$), equation (4.11) is solved to compute $x_N(t_{n+1})$. If $x_N(t_{n+1}) < L$, we add a new interval $(x_N(t_{n+1}), x_{N+1}(t_n))$ in $\mathcal{D}$ with $x_{N+1}(t_n) = L$ and then set $N = N + 1$.

— (**Solve the stationary problem in detached regions and update the right points**.) Solve the stationary elastic problem (2.15) to obtain the profile $\tilde{h}(s, t_{n+1})$ and $\tilde{\gamma}(s, t_{n+1})$ in each detached region $I_i^n = (x_i(t_{n+1}), x_{i+1}(t_n))$ in $\mathcal{D}$ (for odd i) by the method proposed in the §4.1. The value of $\gamma^{n+1}(x_i(t_{n+1}))|_{I_{i-1}}$ in the left neighbouring attached region is used in the boundary condition at x_i. The profile of the sheet may lead to a new detached region $(x_i(t_{n+1}), x_{i+1}(t_{n+1}))$ with $x_{i+1}(t_{n+1}) \in (x_i(t_{n+1}), x_{i+1}(t_n)]$.

— (**Update the profile**.) Update the configuration of the thin sheet by setting

$$\mathcal{A} = \{(x_i(t_{n+1}), x_{i+1}(t_{n+1})) \mid \text{for even } i\}$$

and

$$\mathcal{D} = \{(x_i(t_{n+1}), x_{i+1}(t_{n+1})) \mid \text{for odd } i\}.$$

6. Numerical experiments

In this section, we will use the proposed elastic model and numerical schemes to study the sliding gel problem.

(a) Numerical tests for a stationary problem

We first consider a stationary problem (2.15) to study the shape of the sheet in a detached region. Consider a sheet with length l and thickness H. We set the shear boundary condition on the left boundary $s = 0$ and use the natural boundary condition on the right boundary $s = l$. The admissible sets of h and γ are given in (2.10) and (2.11), respectively.

We choose different parameters to see how the stationary profile of an elastic thin sheet changes with the parameters. In the system, the parameters include G, $r_g = \rho g$, the length of the sheet l, the thickness H and γ_0 for the left boundary condition that $\gamma = \gamma_0$ on $s = 0$. In our experiments, we assume H is much smaller than l. We fix $H = 0.01$ and $l = 0.2$. We solve the problem (2.15) by the numerical method proposed in §4.1.

In the first experiment, we will check the numerical convergence of the numerical method. We set $r_g = 0.01$, $G = 0.1$ and $\gamma_0 = 1.5$. Here γ_0 is used in the left boundary condition that $\gamma(0) = \gamma_0$. We choose different spatial step sizes Δs. Some typical numerical results are shown in figure 6. We can see that solution of height function h and the shear γ converges upon the decreases of the spatial step size. It seems that the convergence of the shear function $\gamma(s)$ is faster than that of $h(s)$.
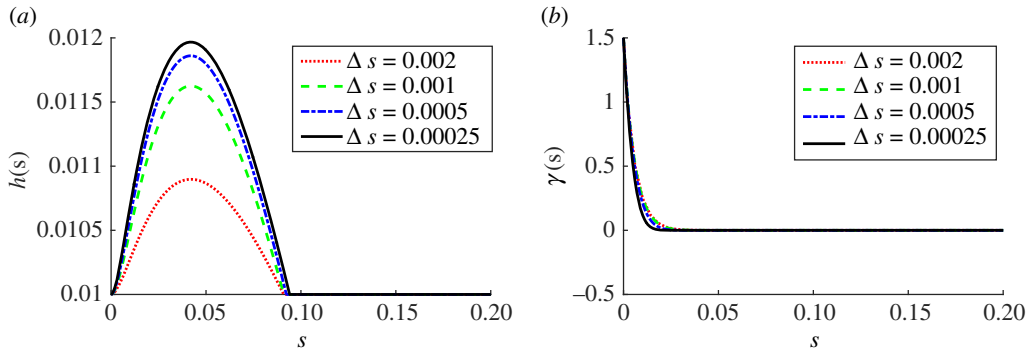
Figure 6. (*a,b*) Convergence tests for the deformation of a detached sheet. (Online version in colour.)

We could also see that only the left part of the sheet is detached from the substrate. The width of the detached region seems not to be sensitive to the spatial step size. The change of γ is dramatic in a layer near the left boundary. The width of the layer is much smaller than the width of the detached region.

We then test how the boundary condition affects the profile of the detached thin sheet in equilibrium. We change only the shear γ_0 in the left boundary condition while keeping all other parameters unchanged. The numerical results are shown in figure 7. In the left column, we show the profile of the thin sheet. The thickness of the sheet is 0.01 which is also shown in the picture. When $\gamma_0 = 1.5$, as shown above, only a part of the sheet detaches from the substrate, due to the gravity of the thin sheet. With the increase of γ_0, the length of the detached region increases. The height of the deformed part also increases slightly. When $\gamma_0 = 2.5$, the whole sheet detaches from the substrate. The results are consistent with the physical understanding of the problem. When the shear strain increases on the left boundary, the sheet will detach more from the substrate. We also tested how the shape of the detached sheet is affected by the elastic parameter G and the density ρ. The profile of the sheet and the changes of $\gamma(s)$ are similar to that in figure 7. Numerical results show that the length of the detached region will increase when we increase the value of G or decrease ρ.

(b) The dynamic problem

We then consider the dynamic sliding of a elastic sheet on the substrate, which is more interesting than the stationary problem. As shown in figure 1, the elastic sheet is fixed on the left end. We suppose the length of the thin sheet is L. The substrate moves rightward in a velocity of v. We use the dynamic model proposed in §3 and the numerical method in the last section to study the problem.

In the experiments we set $H = 0.01$, $r_g = 0.01$, $G = 0.1$ and $\xi = 1$. The critical shear stress (σ in equation (4.11)) is set to be $\sigma = 0.1$. We do experiments for problems with different length L and substrate velocity v_w. Some typical numerical results are shown in figure 8. In these experiments, we set $L = 1$ and $v_w = 0.01$. In a first stage, the thin sheet keeps attached with the substrate while the shear strain γ increases with time as described by Equation (4.3). When the shear stress is larger than some critical value, the detachment occurs first in the right end. The start of the detachment occurs when $t = 1.42$. This is consistent with the analysis below. By (4.3), we know that $d\gamma(s, t)/dt = v_w/H = 1$. Initially, $\gamma(s, 0) = 0$ for all $s \in [0, L]$. Then $\gamma(s, t) = t$ in the early stage. Therefore, the critical time is when $G\gamma(L, t)^2/2 \approx \sigma$ and given by $t = \sqrt{2\sigma/G} \approx 1.414$.

Once the detachment occurs, a bubble gradually forms and moves in the left direction, which is opposite to the velocity of the substrate. The detached region moves in a wavelike way. This is consistent qualitatively with the experimental observations in [18]. Interestingly, our numerical experiments show that the size of the detached region may increase slightly when it moves
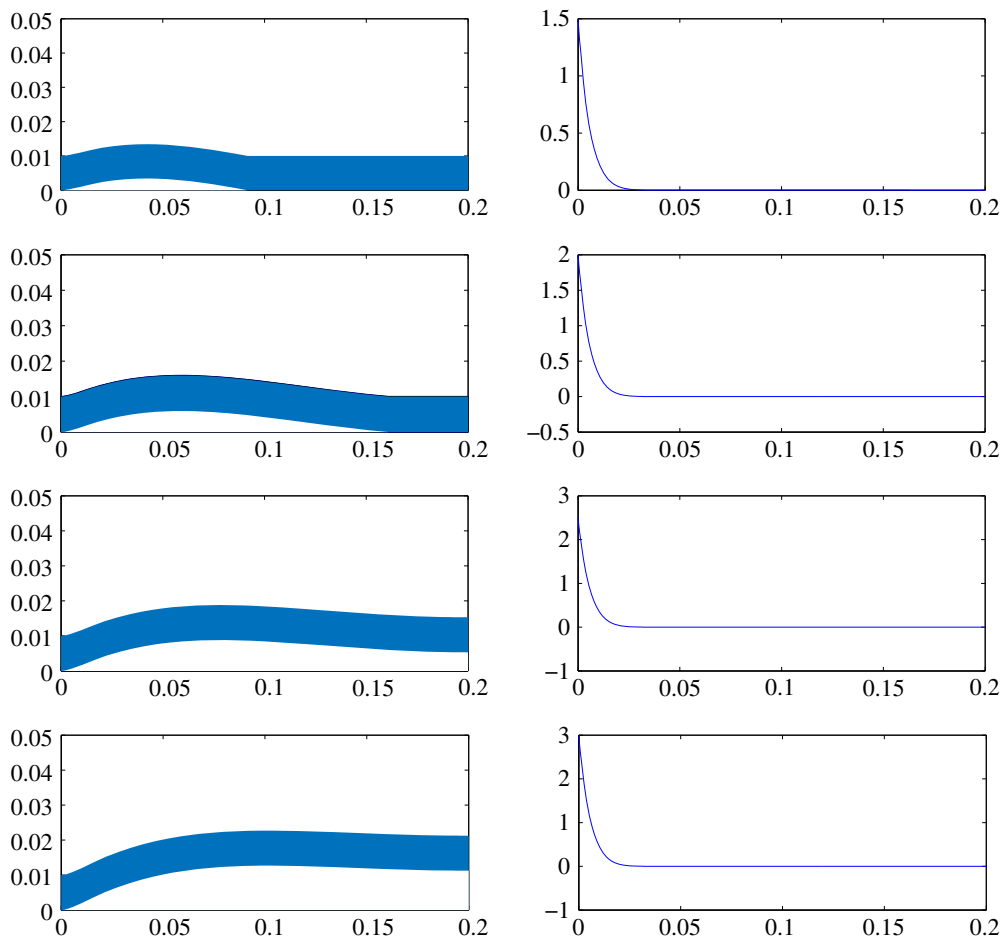
Figure 7. The deformation of a thin sheet with different boundary conditions $\gamma_0 = 1.5, 2, 2.5$ and 3 (from top to bottom). The left column shows the shapes of the thin sheet and the right column shows the shear $\gamma(x)$ in the sheet. (Online version in colour.)

towards the left. This is reasonable, since the shear stress in the left side of the detached region keeps increase when the detached point moves. We notice that when the bubble arrives at the left end, it disappears and the whole sheet attaches again to the substrate again. Later on, a new bubble will appear in the right end and moves left. The process repeats again and again. It looks like a stick–slip behaviour. But the sheet does not slip on the substrate. It releases the energy though the motion of the detached regions which looks like a wave. We also find that the process becomes periodic in time gradually. The early stage is not periodic due to the effect of the initial conditions.

We can also study how the velocity of the detached bubble depends on the velocity of the substrate. We did experiments for the case $L = 1$ under various wall velocities. Notice that the velocity of a bubble is not constant when it moves from right to left. However, since the process is periodic in time, we could compute the average velocity of a bubble in one time period. We denote the velocity as V_{wave} and the wall velocity as v_w. Their relation is shown in figure 9. Numerical results shows that V_{wave} increases when the wall velocity increases with the power law $V_{\text{wave}} \approx v_w^{5/8}$. The result is similar to the experimental results $V_{\text{wave}} \approx v_w^{6/8}$ in [18]. The difference between the numerical results and experiments can be caused by some issues. One key reason is that we choose $\alpha = 2$ in the release rate of the energy in (4.6), which may be not the same as
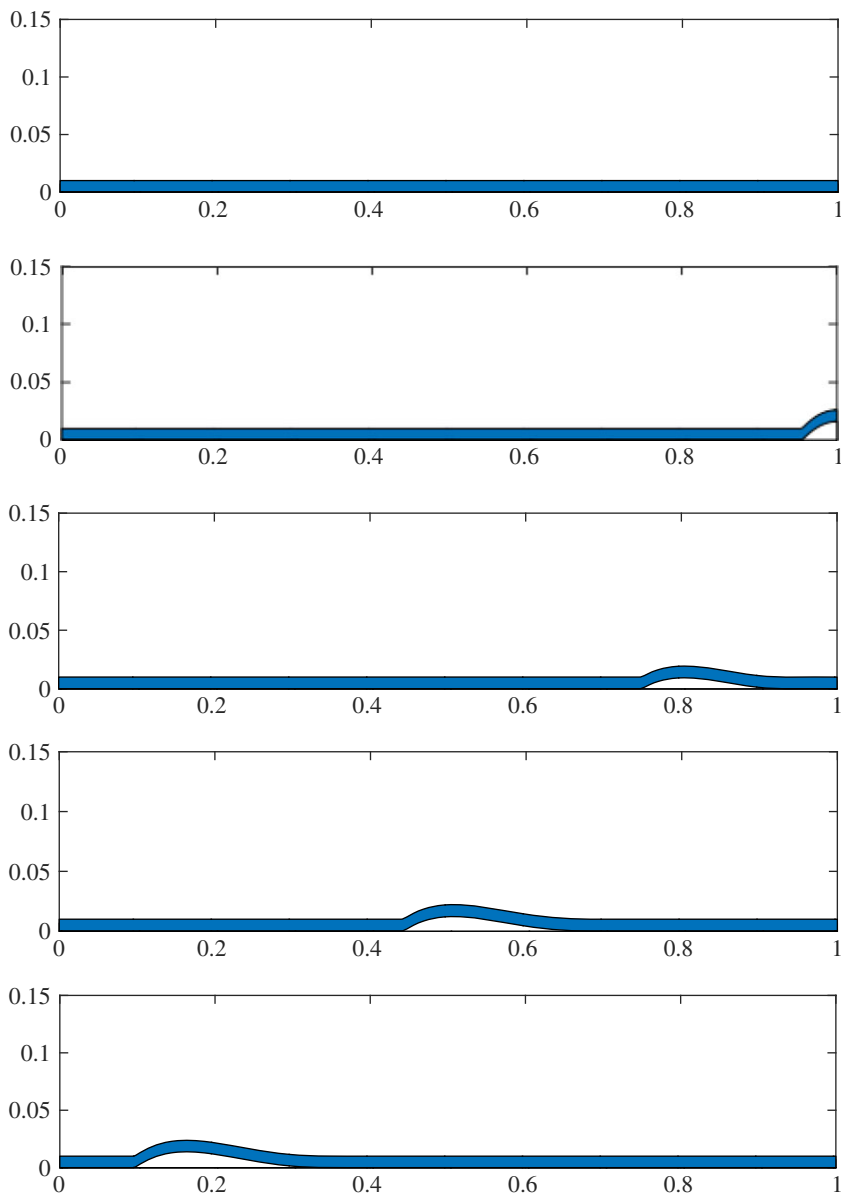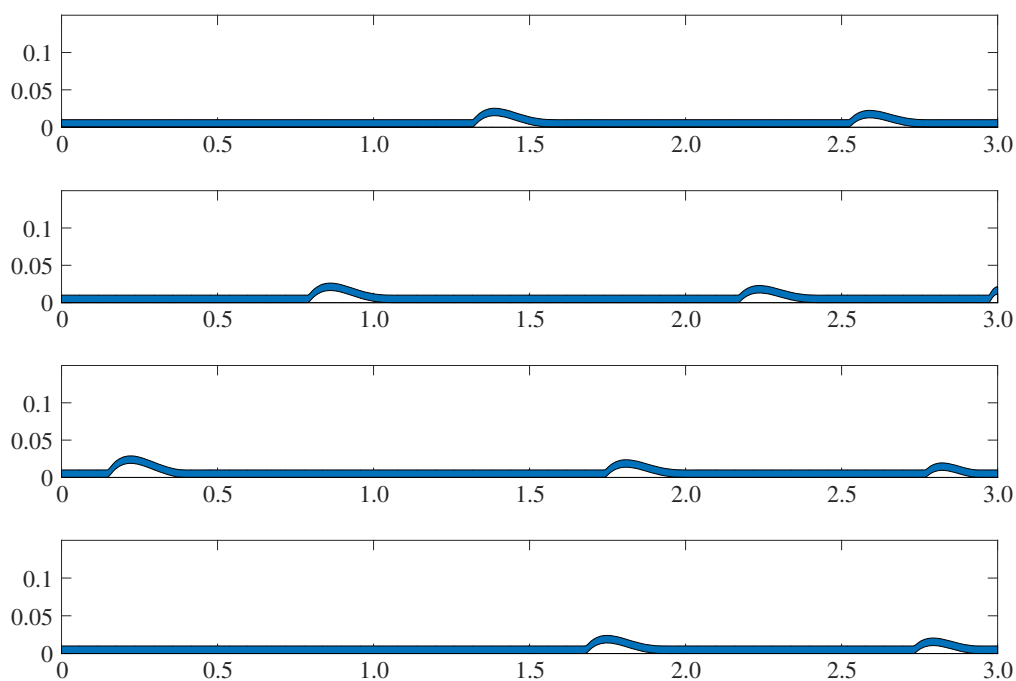
Figure 8. The deformation of a thin sheet with length $L = 1$ and $v = 0.01$ at different times $t = 1, 1.7, 2, 2.25, 2.45$. (Online version in colour.)

that in experiments. Another typical example is shown in figure 10. In this example, we consider a longer sheet with length $L = 3$ and set $v_w = 0.05$. All other parameters are the same as before. In this case, two bubbles of detached regions are observed. There are two factors to make this happen. Firstly, the sheet is long enough so that the stress in the right end increases again from zero to the critical value σ when the first bubble still exists. In this case, a new bubble will form and start to move following the first one. Secondly, the larger velocity of the substrate will make the shear stress increase faster and this also accelerates the process to generate a new bubble.

Numerical results show that the velocity of a bubble increases when it moves to the left. Once again, this is because the shear stress on the (left) detached point becomes larger during the motion of the bubble. By equation (4.11), the detached point will move faster. By this reason, the
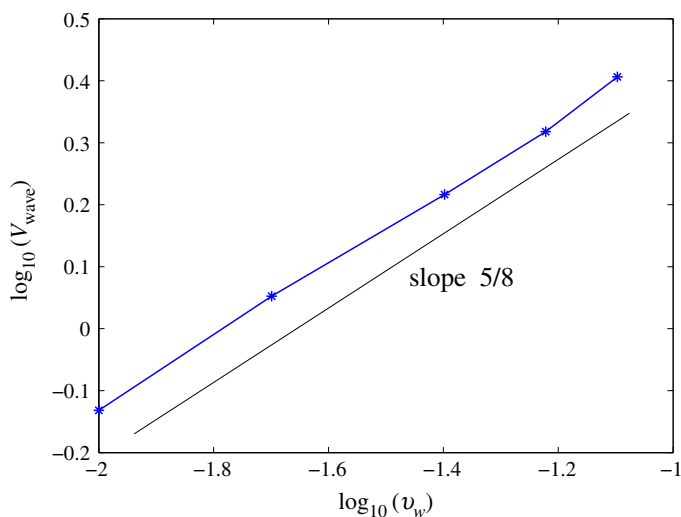
Figure 9. The relation between the average velocity of the detached bubble V_{wave} and the wall velocity v_w. (Online version in colour.)

Figure 10. The deformation of a thin sheet with length $L = 3$ and $v = 0.05$ at different time $t = 5.23, 5.40, 5.86, 5.89$. (Online version in colour.)

distance between the two bubbles increases when they move left. The motion of the two bubbles seems also periodic in time in the later stage. However, there seems to be no steady state since the velocity of the bubbles increase when they move left on the substrate. In figure 11, we show how the number of detached regions increases when the length of the sheet and the substrate velocity
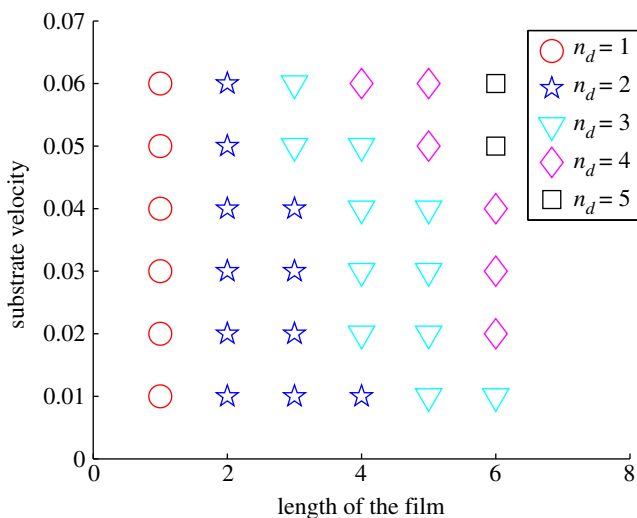
Figure 11. The number of the detachment regions(n_d) for sheets with different length under different substrate velocities. (Online version in colour.)

change. We could see that the number increases when the length of the sheet or the substrate velocity increases. This is consistent with the physical intuition.

7. Conclusion

We develop a mathematical model for the sliding gel sheet on a moving substrate. The model is based on a reduced elastic model for a thin sheet with inextensible upper surface. The Onsager principle is used to study the dynamics of the sliding sheet. Numerical methods are developed to solve both the equilibrium and dynamic problems. Numerical examples show that the model captures the essential phenomena of the sliding gel sheet observed in physical experiments. The Schallamach wave can be clearly seen: when the substrate moves, the detached regions move in an opposite direction. The scaling of the wave velocity with respect to the substrate velocity is consistent with the experimental results. Moreover, numerical results show that the number of waves can be affected by both the length of the sheet and the substrate speed. The reduced model is a one-dimensional model for the thin sheet. It can be generalized to the two-dimensional case which can be used to study the stochastic to regular transition [19]. This will be left for future work.

References

1. Moore DF. 1972 *The friction and lubrication of elastomers*. Oxford, UK: Pergamon Press.
2. Persson B. 2013 *Sliding friction: physical principles and applications*. New York, NY: Springer.
3. Carlson JM, Langer JS. 1989 Properties of earthquakes generated by fault dynamics. *Phys. Rev. Lett.* **62**, 2632–2635. (doi:10.1103/PhysRevLett.62.2632)
4. Roberts AD, Jackson SA. 1975 Sliding friction of rubber. *Nature* **257**, 118–120. (doi:10.1038/257118a0)
5. Briggs G, Briscoe B. 1976 Effect of roughness on rubber friction when waves of detachment are present. *Nature* **262**, 381–382. (doi:10.1038/262381a0)
6. Savkoor A, Briggs G. 1977 The effect of tangential force on the contact of elastic solids in adhesion. *Proc. R. Soc. Lond. A* **356**, 103–114. (doi:10.1098/rspa.1977.0123)
7. Best A, Meijers P, Savkoor AR. 1981 The formation of Schallamach waves. *Wear* **65**, 385–396. (doi:10.1016/0043-1648(81)90064-8)
8. Persson B. 2001 Theory of rubber friction and contact mechanics. *J. Chem. Phys.* **115**, 3840–3861. (doi:10.1063/1.1388626)
9. Baumberger T, Caroli C, Ronsin O. 2002 Self-healing slip pulses along a gel/glass interface. *Phys. Rev. Lett.* **88**, 075509. (doi:10.1103/PhysRevLett.88.075509)
10. Vorvolakos K, Chaudhury MK. 2003 The effects of molecular weight and temperature on the kinetic friction of silicone rubbers. *Langmuir* **19**, 6778–6787. (doi:10.1021/la027061q)
11. Saintyves B, Jules T, Salez T, Mahadevan L. 2016 Self-sustained lift and low friction via soft lubrication. *Proc. Natl Acad. Sci. USA* **113**, 5847–5849. (doi:10.1073/pnas.1525462113)
12. Breki A, Nosonovsky M. 2018 Ultraslow frictional sliding and the stick-slip transition. *Appl. Phys. Lett.* **113**, 241602. (doi:10.1063/1.5064820)
13. Schallamach A. 1971 How does rubber slide. *Wear* **17**, 301–312. (doi:10.1016/0043-1648(71)90033-0)
14. Anooshehpoor A, Brune J. 1994 Frictional heat generation and seismic radiation in a foam rubber model of earthquakes. *Pure Appl. Geophys.* **142**, 735–747. (doi:10.1007/BF00876062)
15. Rubio M, Galeano J. 1994 Stick-slip dynamics in the relaxation of stresses in a continuous elastic medium. *Phys. Rev. E* **50**, 1000–1004. (doi:10.1103/PhysRevE.50.1000)
16. Ronsin O, Baumberger T, Hui CY. 2011 Nucleation and propagation of quasi-static interfacial slip pulses. *J. Adhes.* **87**, 504–529. (doi:10.1080/00218464.2011.575342)
17. Barquins M. 1985 Sliding friction of rubber and Schallamach waves–a review. *Mater. Sci. Eng.* **73**, 45–63. (doi:10.1016/0025-5416(85)90295-2)
18. Yamaguchi T, Ohmata S, Doi M. 2009 Regular to chaotic transition of stick–slip motion in sliding friction of an adhesive gel-sheet. *J. Phys.: Condens. Matter* **21**, 205105. (doi:10.1088/0953-8984/21/20/205105)
19. Morishita M, Kobayashi M, Yamaguchi T, Doi M. 2010 Observation of spatio-temporal structure in stick–slip motion of an adhesive gel sheet. *J. Phys.: Condens. Matter* **22**, 365104. (doi:10.1088/0953-8984/22/36/365104)
20. Onsager L. 1931 Reciprocal relations in irreversible processes. I. *Phys. Rev.* **37**, 405–426. (doi:10.1103/PhysRev.37.405)
21. Onsager L. 1931 Reciprocal relations in irreversible processes. II. *Phys. Rev.* **38**, 2265–2279. (doi:10.1103/PhysRev.38.2265)
22. Doi M. 2013 *Soft matter physics*. Oxford, UK: Oxford University Press.
23. Doi M. 2011 Onsager's variational principle in soft matter. *J. Phys.: Condens. Matter* **23**, 284118. (doi:10.1088/0953-8984/23/28/284118)
24. Creton C, Ciccotti M. 2016 Fracture and adhesion of soft materials: a review. *Rep. Prog. Phys.* **79**, 046601. (doi:10.1088/0034-4885/79/4/046601)
25. Xu X, Calderer MC, Doi M, Henao D. 2020 Source codes for debonding waves in gel thin films. (doi:10.5281/zenodo.3895746)